U. Walzer, R. Hendel.Real episodic growth of continental crust or artifact of preservation? A 3-D geodynamic model.
J. Geophys. Res., 118, doi:10.1002/jgrb.50150, 2013.

Real episodic growth of continental crust or artifact of preservation? A 3-D geodynamic model

Uwe Walzer[1] and Roland Hendel[1]

Received 8 June 2012; revised 4 March 2013; accepted 7 March 2013.

[1] We investigate whether the observed zircon age distribution of continental crust (CC) is produced by real crustal growth episodes or is only an artifact of preservation. In connection with the second alternative of this question, other authors proposed that there was little episodicity in the production of new CC and that modeling corroborates this opinion. We conclude that a combination of the two answers might be possible. In matters of modeling, however, we ascertain that a *dynamic* modeling of the convection-differentiation system of the mantle reveals the high probability of magmatic episodes. We solve the full set of balance equations in a 3-D spherical-shell mantle. The heat-producing elements are redistributed by chemical differentiation. A realistic solidus model of mantle peridotite is essential for an applicable model. The solidus depends not only on depth but also on the volatile concentration. Furthermore, we introduced realistic profiles of Grüneisen parameter, viscosity, adiabatic temperature, thermal expansivity, and specific heat. Our model automatically produces lithospheric plates and growing continents. Regarding number, size, form, distribution, and surface velocity of the continents, no constraints have been prescribed. Regions of the input parameter space (Ra, σ_y, k, f_3) that are favorable with respect to geophysical quantities show *simultaneously* not only episodicity of CC growth but also a reproduction of the observed zircon-age maxima referring to the instants of time. We also obtain Archean events for ages greater than 3000 Ma that are not or scarcely visible in the observed zircon ages. Sinusoidal parts of the evolution curve of *qob*, *Ur*, and E_{kin} are superposed with a monotonous decrease. The volumetrically averaged mantle temperature, T_{mean}, however, decreases smoothly and slowly, nearly without pronounced variations. Therefore, we can dismiss catastrophic mechanisms that *simultaneously* incorporate the *whole* mantle.

Citation: Walzer, U., and R. Hendel (2013), Real episodic growth of continental crust or artifact of preservation? A 3-D geodynamic model, *J. Geophys. Res. Solid Earth*, *118*, doi:10.1002/jgrb.50150.

1. Introduction

1.1. Conception

[2] The hypsometric curve of the Earth is bimodal. In our planetary system, this fact is unique. The existence of oceans at the surface of the solid Earth is unique, too. It is an obvious guess that the two unique features have a causal connection. The upper continental crust (UCC) is felsic, rich in Si, poor in Mg, and enriched in incompatible elements. The oceanic crust, however, is poor in Si, rich in Mg, and not as highly enriched in incompatible elements as UCC, both in comparison to "mantle reservoirs." We use the concept of reservoirs considerably different than in former time. We mean it similarly as defined by *Stracke et al.* [2005] and *Willbold and Stracke* [2006]. We do not imagine sharp boundaries between mantle reservoirs. We use this concept only as a simple tool to describe the evidently rather inhomogeneous Earth's mantle. We define the chemical composition of a specific mantle location by the mixing ratio of the conventional reservoirs [*Hofmann*, 2003]. The exact chemical composition of the bulk continental crust (CC) is controversial. *Taylor and McLennan* [1985, 1995, 2009] assume a composition between andesitic and basaltic-andesitic with slightly more than 57 wt% SiO_2, whereas *Rudnick and Fountain* [1995] and *Rudnick and Gao* [2003] deduced an andesitic mean composition with about 60 wt% SiO_2 and elevated K_2O values. *Wedepohl* [1995] proposed a high-K andesitic model with over 62 wt% SiO_2. It is irrefutable that some alkali elements are highly enriched in comparison with the primordial mantle, regardless if we assume a chondritic mantle as usual or a nonchondritic mantle [*Caro*, 2011] as a starting composition. Furthermore, we observe a complementary depletion in a part of the mantle called depleted MORB mantle (DMM) which evidently can be found at least immediately beneath ocean

[1]Institut für Geowissenschaften, Friedrich-Schiller-Universität, Jena, Germany.

Corresponding author: U. Walzer, Institut für Geowissenschaften, Friedrich-Schiller-Universität, Humboldtstr. 11, 07743 Jena, Germany. (u.walzer@uni-jena.de)

2169-9313/13/10.1002/jgrb.50150

lithosphere. In addition, it is evident that the mid-oceanic ridge basalt (MORB) is a product of the chemical differentiation of DMM [*Hofmann*, 1988, 2003; *Davidson and Arculus*, 2006]. There are at least five models of the generation of CC which differ considerably [*Davidson and Arculus*, 2006]. The growth rate of the CC is a function of the balance between addition of mantle material by chemical differentiation in several steps and the loss of CC back into the mantle by subduction of continental sediments, subduction erosion, and lower crust delamination [*Condie*, 1998; *Condie and Aster*, 2010; *Clift et al.*, 2009; *Hawkesworth et al.*, 2010; *Stern and Scholl*, 2010; *Roberts*, 2011]. It is remarkable that the lower CC delamination generates nearly no loss of UCC which has a rather high percentage of Si, alkali elements, U, Th, and other incompatible elements.

[3] Well-crystallized zircon, $ZrSiO_4$, preserves the isotopic ratios that stem from the date of origin of a magmatic rock. Therefore, zircon methods should better represent the original process of chemical differentiation than whole-rock isotopic systems. *Condie and Aster* [2010] investigate a very large database of 8928 orogenic granitic and 28,027 detrital U/Pb zircon ages and apply a kernel density analysis. Using a kernel bandwidth of 90 Ma, they identify four principal maxima that are situated at about 2686, 1871, 576, and 1073 Ma if arranged according to their height. One conclusion is that at least 60% of the juvenile CC already exists at an age of τ = 2600 Ma. *Hawkesworth and Kemp* [2006] emphasize that Hf isotopes excellently reflect when new crust is generated from the mantle. They note that Hf ages of zircons with mantle-like $\delta^{18}O$ values fall into two age ranges, namely 1.7–1.9 Ga and 2.9–3.1 Ga. Other peaks are interpreted by crustal differentiation. They conclude that much of the CC was generated during these two pulses of relatively rapid growth. In anticipation of our results, we remark that it is not our aim to comparatively evaluate the observational results of other authors but to numerically derive a physically consistent theory of CC generation, in connection with other geodynamic phenomena. It is, however, remarkable that we *simultaneously* obtain the CC production maxima of *Condie and Aster* [2010] and of *Hawkesworth and Kemp* [2006] by a group of runs, the input parameters of which are physically plausible for entirely other reasons.

[4] Prior papers on CC generation assume slow-growth models with very little CC formation before 4 Ga [*Veizer and Jansen*, 1979; *Patchett and Arndt*, 1986; *McCulloch and Bennett*, 1993, 1994; *Taylor and McLennan*, 1995]. Models of this kind often show steep gradients in the growth curves [e.g., *Taylor and McLennan*, 1995; *Condie and Aster*, 2010]. Many authors interpreted these steep gradients as periods of high generation of juvenile CC stemming from the mantle. The mentioned observations are not obsolete, also today, but require a lucid physical explanation. Additionally, new observations appeared which refer to Hadean and Archean.

[5] The Earth accreted about 4565 Ma. Undoubtedly, the mantle was in magma ocean stage during that time. *Harrison et al.* [2005] measured $^{176}Hf/^{177}Hf$ initial ratios of 4.01 to 4.37 Ga detrital zircons. *Harrison et al.* [2008] extended this investigation using concurrent Lu-Hf and $^{207}Pb/^{206}Pb$ analyses and deduced model ages between 4.56 and 4.20 Ga for the extraction of the zircon's protoliths. They concluded that already by 4.35 Ga, sialic crust had begun to form. Outside Western Australia, *Iizuka et al.* [2006] found U-Pb zircon age estimates of 4.2 Ga in a 3.9 Ga granitic rock in the Acasta Gneiss Complex of Canada. They concluded that the 3.9 Ga granitic magma was derived from a 4.2 Ga CC. *Zheng and Zhang* [2007] report Hf model ages of 4.0 Ga in South China and a 4.1 Ga U-Pb age of a detrital zircon found in Tibet. Furthermore, they show distinct cumulative peaks of micro-scale U-Pb dates of zircons from South China that are older than 2.7 Ga and their observed frequency decreases with growing age. This could possibly indicate that the same mechanism which generates the peaks shown by *Hawkesworth and Kemp* [2006] and *Condie and Aster* [2010] has already been effective earlier. Because tectonically active periods of time show not only differentiation of juvenile crust but also reworking of available CC, the amount of preserved Archean CC should decrease with age. *Blichert-Toft and Albarède* [2008] investigated 63 single zircons from Jack Hills, Western Australia, which were formed during a single magmatic pulse 4.1 ± 0.1 Ga ago, and that were derived from a 4.30 to 4.36 Ga old protolith. The $^{176}Lu/^{177}Hf$ ratios fit a tonalite-trondhjemite-granodiorite (TTG) source. *Guitreau et al.* [2012] examined whole-rock and zircon MC-ICP-MS Lu-Hf isotope date of Archean TTGs. The $^{176}Lu/^{177}Hf$ ratio of the mantle source of CC is nearly constant in a scatterplot between 0.032 and 0.038 since about 3.9 Ga, whereas the chondritic value of this ratio is 0.0336. They argue that these data and other observations support the (perhaps stepwise) derivation of CC from a primitive, possibly chondritic mantle. From results of the Jack Hills zircons, they conclude that the mantle source of continents has remained unchanged since 4.3 Ga. The discussed papers contain strong indications of peaks of CC production before the pronounced maximum at 2.7 Ga, which are largely hidden by later processes.

[6] The DMM is thought to be the residue of some preliminary mode of CC. On the other hand, DMM is considered to be the source of MORB. The percentage of prior melt extraction from the primordial mantle is controversial. Estimates range from 30% to 100% according to the method and the authors [*O'Nions et al.*, 1979; *Zindler and Hart*, 1986; *Hofmann*, 1997; *Boyet and Carlson*, 2006; *Stracke et al.*, 2011]. Here we develop a numerical convection-differentiation mantle model of chemical and thermal evolution, on reliable physical foundations, to strike a balance between the reviewed doctrines. So we do not intend to add entirely new geochemical or isotopic arguments, but we want to show that a physically sound model is feasible and that it confirms and explains essential geochemical and geological findings.

1.2. Other Proposed Mechanisms

[7] There are some different proposals to explain the episodic distribution of zircon dates and other undisputed observations. It is well known that some present-day subducting slabs are transiently retained over and parallel to the 660 km discontinuity [*van der Hilst et al.*, 1997]. From this, some models of catastrophic slab avalanches, flashes, and sudden convective overturns have been developed that are thought to result in more rapid movements of lithospheric plates near the surface. Also, *O'Neill et al.* [2007; 2008] interpret the age peaks (e.g., at 1.1, 1.9–2.1, 2.7, and 3.5 Ga) as maxima of increased CC production. They emphasize that in some cases, ^{40}Ar and ^{18}O isotopic data argue against

a strong CC recycling into the deep mantle. They support the opinion that juvenile CC generation is episodic and propose a mechanism with strongly time-dependent subduction under the hotter conditions of the Precambrian mantle. They hypothesize repeated breakdowns of continuous plate tectonics induced by the balancing of driving convective stresses with resistive plate strengths. *Davies* [2007, 2008] emphasizes that subducted oceanic crust is buoyant between 660 and 750 km depth. The slab lingers for some time and finally subducts into the lower mantle. During such periods of impeded subduction, the upper mantle cools and the lower mantle warms. Every 100 to 150 Ma, this mechanism results in a magmatic episode. No subsequent layering occurs after about 1.6 to 1.8 Ga in Davies' model. Evidently, the last-mentioned two models cannot explain the magmatic episodes during the Phanerozoic. Furthermore, a realistic balancing of the number of atoms of a specific atomic species in the reservoirs will succeed only in a 3-D spherical-shell model with considerably more grid points; however, the last-mentioned two models are two-dimensional and Cartesian. Nevertheless, the two models contain important features of an overall convection mechanism.

[8] A linkage between plumes and magmatic episodicity has been proposed by other authors. *Nolet et al.* [2007] proved that at least some plumes ascend from the core-mantle boundary (CMB). Because of the high viscosity in the middle part of the lower mantle (cf. Figure 3), the lateral velocity of plumes is low in comparison to the velocities of oceanic lithospheric plates. Therefore, the distribution of ages of volcanoes in plume-related volcanic chains can serve to estimate the plate velocities and to corroborate the results from the spreading-rate-dependent magnetization of the oceanic lithosphere. Large igneous provinces (LIPs) are divided into three classes: continental flood basalts, oceanic plateaus, and ocean basin flood basalts [*Coffin and Eldholm*, 1994]. The latter two classes of LIPs are carried by the conveyor-belt-like oceanic lithosphere and are accreted to continents in zones of andesitic volcanism. One group of models assumes that this type of continental crustal growth is dominant [*Stein and Hofmann*, 1994; *Abbott et al.*, 1997; *Albarède*, 1998]

[9] *Hawkesworth et al.* [2010] propose another view. They accept that zircons yield precise crystallization ages. However, they argue that the peaks of relative frequency of zircon age estimates above the axis of time are not a direct record of increased magmatic activity but an artifact of preservation. The formation of a supercontinent would cause an elevated preservation potential [*Hawkesworth et al.*, 2009]. Similarly, *Belousova et al.* [2010] conclude from a database of about 13,800 U-Pb and Hf-isotope analyses of zircons that there is little episodicity in juvenile CC growth in contrast to peaks in magmatic ages. They propose that these magmatic peaks originate from supercontinent formation.

[10] *Gurnis and Davies* [1986] realized that the curves of CC growth are the same as crustal-age distributions only if there is no recycling of CC back into the mantle. Unfortunately, the assessments on the percentage of recycled CC are unreliable. The UCC will be removed down to the mantle probably only by subduction of UCC sediments and by lateral erosion by downgoing oceanic lithosphere, but not by delamination or foundering. *Gurnis and Davies* [1986] note that the physics of convection *strongly inhibit rapid changes in the mean temperature of the mantle*. Our numerical investigations clearly confirm this conclusion. This implies that, according to our numerical results, no disastrous *whole-mantle* movements are to be expected. However, we can show that using very moderate physical assumptions, real episodic growth of the continental crust is possible and most likely and that the observed temporal distribution of magmatic episodes is consistent with computed episodes.

[11] As an introduction to the solid-state convection of the mantle, we refer to *Schubert et al.* [2001]. Regarding thermochemical mantle convection, we mention *Nakagawa and Tackley* [2004] and *Ogawa* [2008].

2. Model Description

[12] Our numerical model is based on the assumption that the augmented preservation potential [*Hawkesworth et al.*, 2009, 2010; *Belousova et al.*, 2010 is *also* associated with the complete convection-differentiation system by the generation of supercontinents. This system determines, in principle, also all other special mechanisms that have been proposed to explain the episodes of increased magmatism. Therefore, we want to design a rather general, physically acceptable numerical model where plates and plumes are not prescribed but can self-consistently develop and are an integral part of the numerical model. The seemingly alternative modes of (a) early growth of continental crust and subsequent recycling *or* (b) continuous crustal growth *or* (c) episodic crustal growth are also not prescribed but appear as a solution of the system of balance equations. We use a similar approach with respect to the continents. Our model continents are not artificially imposed. Neither the number of continents nor their size, form, or position are prescribed. The growing function of total continental mass is not presupposed, too. The last named parameters evolve from the differential equations of convection and some simplified equations of chemical differentiation with a physically reasonable starting criterion of chemical differentiation. Expectedly, we found an interplay between convection/mixing and differentiation.

2.1. Balance of Mass, Energy, and Momentum

[13] We developed a model of the Earth's thermal and chemical evolution for the whole time span. The thermal evolution of the core is taken into account only in a parameterized way. We use a numerical strategy for modeling the chemical differentiation leading to the juvenile contributions that are added to the continents. In a similar manner, we computed the mixing processes between the depleted mantle and the other (chemically inhomogeneous) parts of the mantle. We solve the differential equations of infinite Prandtl number convection using a three-dimensional finite-element spherical-shell method. These equations express the conservation of mass, energy, and momentum. For the *mass balance*, we use the anelastic liquid approximation

$$\nabla \cdot \vec{v} = -\frac{1}{\rho}\vec{v} \cdot \nabla \rho \qquad (1)$$

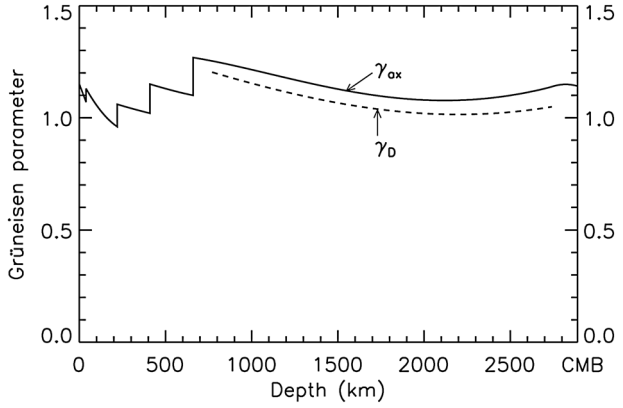

Figure 1. A comparison of different Grüneisen parameters, γ, as a function of depth, h. The extended acoustic gamma is denoted by γ_{ax}, the Debye gamma by γ_D.

where $\vec{v}$ is velocity and ρ is density. The energy balance can be expressed as

$$\frac{\partial T}{\partial t} = -\frac{\partial (T v_j)}{\partial x_j} - (\gamma - 1) T \frac{\partial v_j}{\partial x_j} + \frac{1}{\rho c_v}\left(\tau_{ik}\frac{\partial v_i}{\partial x_k} + \frac{\partial}{\partial x_j}\left(k\frac{\partial}{\partial x_j}T\right) + Q\right] \quad (2)$$

where T denotes the temperature, t the time, v_j and x_j the components of the creep velocity and the location vector, respectively, γ the Grüneisen parameter, c_v the specific heat at constant volume, k the thermal conductivity, and Q the heat generation rate per unit volume. We have to put the deviatoric stress tensor, τ_{ik}, into (2):

$$\tau_{ik} = \eta\left(\frac{\partial v_i}{\partial x_k} + \frac{\partial v_k}{\partial x_i} - \frac{2}{3}\frac{\partial v_j}{\partial x_j}\delta_{ik}\right) \quad (3)$$

where the shear viscosity, η, is calculated by

$$\eta(r,\theta,\phi,t) = 10^{r_n} \cdot \frac{\exp\left(c\overline{T_m/T_{av}}\right)}{\exp\left(c\overline{T_m/T_{st}}\right)} \cdot \eta_4(r) \cdot \exp\left[c_t \cdot T_m\left(\frac{1}{T} - \frac{1}{T_{av}}\right)\right] \quad (4)$$

[14] The melting temperature, T_m, and therefore the viscosity, strongly depends on the Grüneisen parameter. Furthermore, one important term in the preferred version of the energy balance, equation (2), explicitly depends on the Grüneisen parameter which can be derived directly from seismic observations. Therefore, this approach contains only a minimum of hypotheses on the pressure dependence of material parameters. In (4), r is the radius, θ the colatitude, ϕ the longitude, r_n the viscosity-level parameter, T_{av} the laterally averaged temperature, and T_{st} the initial temperature profile. The quantity $\eta_4(r)$ is the viscosity profile at the initial temperature and $r_n = 0$. The second factor on the right-hand side of (4) describes the increase of the viscosity profile with the cooling of the Earth. For $MgSiO_3$ perovskite we should insert $c = 14$, and for MgO wüstite $c = 10$ according to *Yamazaki and Karato* [2001]. So the lower mantle value of c should be somewhere between these two values. For numerical reasons, we can use only $c = 7$. In the lateral-variability term, we apply $c_t = 1$.

[15] As an *equation of state*, we apply

$$\rho = \rho_r\left[1 - \alpha(T - T_r) + K_T^{-1}(P - P_r) + \sum_{k=1}^{2}\Gamma_k \Delta\rho_k/\rho_r\right] \quad (5)$$

where the index r refers to the adiabatic reference state, $\Delta\rho_k/\rho_r$ denotes the non-dimensional density jump for the kth mineral phase transition. Γ_k is a measure of the relative fraction of the heavier phase where $\Gamma_k = \frac{1}{2}\left(1 + \tanh\frac{\pi_k}{d_k}\right)$ with $\pi_k = P - P_{0k} - c_k T$ describing the excess pressure π_k. The quantity P_{0k} is the transition pressure at zero temperature T. A non-dimensional transition width is denoted by d_k. The quantity c_k represents the Clausius-Clapeyron slope for the kth phase transition. Γ_k and π_k have been introduced by *Richter* [1973] and *Christensen and Yuen* [1985].

[16] The high-Prandtl-number version of the *momentum balance* is

$$0 = -\frac{\partial}{\partial x_i}(P - P_r) + (\rho - \rho_r) g_i(r) + \frac{\partial}{\partial x_k}\tau_{ik} \quad (6)$$

where we have to insert again (3) and (4) as well as a gravity acceleration model for $g_i(r)$, e.g., from preliminary reference Earth model (PREM) [*Dziewonski and Anderson*, 1981]. P signifies the pressure. So the equations (1), (2), (5), and (6) are a system of six scalar equations for the determination of six scalar unknown functions, namely T, ρ, P, and the three creep velocity components v_i. We use the tracer method described in Appendix A of *Walzer and Hendel* [2008] to conserve the sum of the number of atoms of the pairs ^{238}U-^{206}Pb, ^{235}U-^{207}Pb, ^{232}Th-^{208}Pb, and ^{40}K-^{40}Ar, respectively. Our condition of chemical differentiation (cf. section 2.2) is new and differs from the condition used by *Walzer and Hendel* [2008].

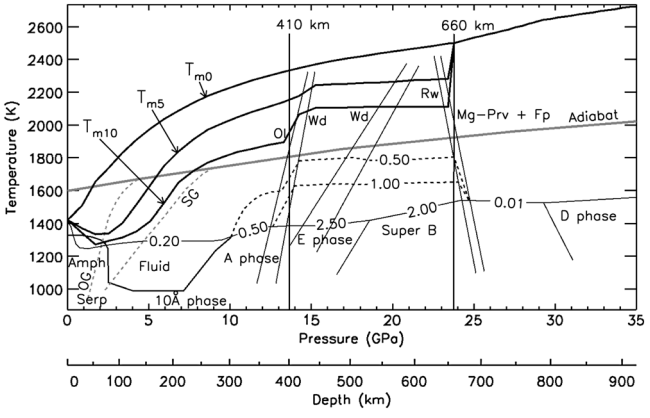

Figure 2. The solidi, T_{sol}, of peridotite as a function of pressure, P, and of the water concentration, modified according to [*Litasov*, 2011]. The curve for 0 wt% H_2O is denoted by T_{m0}, for 0.05 wt% H_2O by T_{m5}, and for 0.10 wt% H_2O by T_{m10}. We computed the continuation of T_{m0} for the deeper mantle using equation (10). The MORB adiabat with a potential temperature of 1588 K is called "Adiabat." Ol, olivine; Wd, wadsleyite; Rw, ringwoodite; Mg-Prv, magnesium perovskite; Fp, ferropericlase.

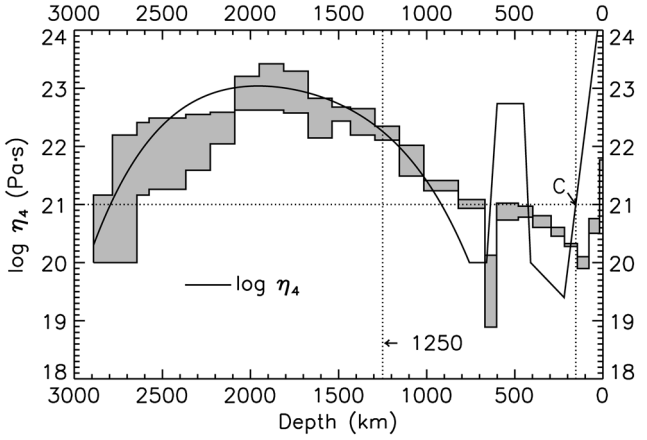

Figure 3. A comparison of our viscosity function η_4 (solid line) with the viscosity profile by [*Mitrovica and Forte*, 2004].

2.2. Material Parameters, Heating, Chemical Differentiation, and Initial and Boundary Conditions

[17] Section 2.1 not only provides the balance equations but shows also which radial profiles of *material parameters* are necessary. Here we present the results and keep the derivation of these parameter profiles very short. The Grüneisen parameter, γ, is very important for solid-state geophysics [*Anderson*, 1995; *Poirier*, 2000; *Stixrude and Lithgow-Bertelloni*, 2007; *Karato*, 2008; *Stacey and Davis*, 2009]. It is physically reasonable to apply only such approximations of γ that we can determine using geophysically observable variables and that contain also the shear modes. Hence, we compare, in Figure 1, the extended acoustic gamma, γ_{ax}, with the Debye gamma, γ_D. We computed both functions between 771 and 2741 km depth using PREM values. The acoustic gamma, γ_a, stems from

$$\gamma_a = \frac{1}{6}\frac{K_T}{K_S + (4/3)\mu}\left[\left(\frac{\partial K_S}{\partial P}\right)_T + \frac{4}{3}\left(\frac{\partial \mu}{\partial P}\right)_T\right] + \frac{1}{3}\frac{K_T}{\mu}\left(\frac{\partial \mu}{\partial P}\right)_T - \frac{1}{6} \tag{7}$$

The Debye gamma, γ_D, has been computed using

$$\gamma_D = \frac{1}{3} - \frac{1}{3}\left[d\ln\left(\frac{1}{v_p^3} + \frac{2}{v_s^3}\right)/d\ln\rho\right] \tag{8}$$

The quantity K_S denotes the adiabatic bulk modulus, K_T the isothermal bulk modulus, μ the shear modulus, and v_p and v_s the velocities of compressional and shear waves, respectively. For physical reasons, we prefer γ_a for our geodynamic computations. Now it would be mathematically convenient to determine γ_a using PREM also for the other depths of mantle and crust. However, some geophysicists, e.g., *Stacey and Davis* [2009], noticed that the seismological PREM estimates of dK/dP and dμ/dP of the upper mantle and crust lead to physically implausible depth variations of γ. Therefore, we use the gamma estimates of *Stacey and Davis* [2009] for the upper parts of the mantle in the range of $h < 771$ km and for the D″ layer. The composite curve is called extended acoustic gamma, γ_{ax}.

[18] We assume that the present-day asthenosphere is in the solid state apart from relatively small magma chambers in the vicinity of mid-ocean ridges and near hot spots. So partial melt is *not* required to explain the physical properties of the present-day seismic low velocity zone [*Karato*, 2008; *Stixrude and Lithgow-Bertelloni*, 2010]. Partial melting in major volumes occurs only when occasionally

$$T > f_3 \cdot T_m \tag{9}$$

applies or when the total H_2O abundance exceeds the H_2O solubility [*Mierdel et al.*, 2007; *Litasov*, 2011] where f_3 is a parameter that is somewhat smaller than or equal to 1 and that we vary in the different Terra runs. We shall indeed show that such kind of regional episodic partial melting really occurs. We assume that if (9) is fulfilled, not only the incompatible elements redistribute according to Table 2 but also a high percentage of water leaves the respective volume of peridotite where the regional solidus value increases (Figure 2). Figure 2 shows the solidus diagram for water-containing peridotite. The estimations of the solidus, $T_{\rm sol}$, for the uppermost lower mantle have been continued down to the whole lower mantle using

$$\frac{1}{T_{\rm sol}} \cdot \frac{{\rm d}T_{\rm sol}}{{\rm d}P} = \frac{2}{K}\left(\gamma_{ax} - \frac{1}{3}\right) \tag{10}$$

where K is the bulk modulus according to PREM. The solid line in Figure 3 shows the quantity $\eta_4(r)$, which describes the viscosity profile at the initial temperature, T_{st}, and for $r_n = 0$. The absolute level of the $\eta_4(r)$ curve is determined in such a way that the volumetric mean of $\log \eta_4(r)$ between C and h = 1250 km is exactly equal to 21, the Haskell value, if η_4 is inserted in Pa s.

[19] For the uppermost 285 km of the mantle (including crust), we implemented an effective viscosity, $\eta_{\rm eff}$, with

$$\eta_{\rm eff} = \min\left[\eta(P,T), \frac{\sigma_y}{2\dot{\varepsilon}}\right] \tag{11}$$

where $\dot{\varepsilon}$ is the second invariant of the strain-rate tensor. The quantity σ_y denotes a viscoplastic yield stress. The introduction of yield stress and the first low viscosity zone above $h = 410$ km (cf. Figure 3) facilitate plate-like motions of the lithosphere. *Yoneda et al.* [2009] assume a thermal conductivity of $k = 5.00$ W/(m K). We, however, vary this parameter from run to run. Also for σ_y in (11), r_n in (4) and f_3 in (9), we prefer a variation of parameters. Finally, we add some material parameters to be able to insert the heat production density, Q, in equation (2).

$$Q = \rho \cdot \sum_{\nu=1}^{4} a_{\mu\nu}\, a_{if\nu}\, H_{0\nu} \cdot e^{-t/\tau_\nu} \tag{12}$$

The quantity Q is temporally variable, not only because of the radioactive decay but also because of the redistribution of abundances, $a_{\mu\nu}$, of the major heat-producing

Table 1. Data of the Major Heat-Producing Isotopes

Isotope	^{40}K	^{232}Th	^{235}U	^{238}U
ν	1	2	3	4
τ_ν (Ma)	2015.3	20212.2	1015.4	6446.2
$H_{0\nu}$ (mW/kg)	0.272	0.0330	47.89	0.1905
$a_{if\nu}$	0.000119	1	0.0071	0.9928

Table 2. The Abundances $a_{\mu\nu}$ of Some Incompatible Elements in ppm

Reservoir Index	BSE (1)	Oceanic Crust (2)	CC (3)	DMM (4)
element				
U	0.0203	0.047	0.94	0.0066
Th	0.0853	0.12	4.7	0.017
K	250.	600.	9460.	110.
Pb	0.1382	0.30	7.0	0.035
Sm	0.4404	2.63	4.62	0.378
Nd	1.354	7.3	25.5	0.992
Rb	0.635	0.56	35.5	0.112
Sr	21.0	90.	310.	16.6

elements due to chemical differentiation. Table 1 presents some parameter data for the four major heat-producing isotopes. The letter ν is the consecutive number of the four major radionuclides, τ_ν is the decay time or the $1/e$ lifetime, $H_{o\nu}$ is the specific heat production of the νth radionuclide 4565 Ma ago, and $a_{ij\nu}$ denotes the isotope abundance factor. We use the *McCulloch and Bennett* [1994] reservoir abundances (cf. Table 2) since they are self-consistent. In spite of this choice, we emphasize that we do *not* use the old concept of chemical mantle reservoirs with distinct separation planes. Only the percentage of a component differs between different locations. So modern reservoirs are only a numerically convenient characterization for a nearly everywhere inhomogeneous Earth's mantle.

[20] We start with a uniform distribution of exclusively type-1 tracers representing a bulk-silicate Earth (BSE) mantle (cf. Table 2). If the computed model temperature, T, approaches the melting temperature, T_m, in a sufficiently large volume, i.e., if the condition of equation (9) is fulfilled, then chemical differentiation occurs. The new CC material will be welded to an existent continent if an oceanic plate has carried it to a continental margin [*Walzer and Hendel*, 2008, Appendix A]. Our present model also incorporates those buoyancy forces that are generated by thermally induced deflections of the phase boundaries of the olivine-wadsleyite transition and of the ringwoodite-perovskite transition.

[21] We prescribe free-slip and impermeable boundary conditions for both the Earth's surface and the CMB. As regards the distribution of continents and oceans at the surface, we do not prescribe anything except that oceanic plateaus (see Figure 8, black areas) have to be aggregated with the continent if the plateau touches the continent. This procedure represents the accretion of terranes. The upper surface of the mantle is temporally and spatially isothermal at 288 K. The CMB is also isothermal. However, the CMB temperature, T_c, is a function of time applying a cooling core-mantle evolution model [*Steinbach et al.*, 1993]. We adjust T_c after each time step according to the heat flow through the CMB. In a cooling mantle, T_c must decrease.

3. Results

[22] Figure 4 shows that run 498 with $r_n = 0.5$ (which corresponds to $Ra \approx 10^8$) and $\sigma_y = 120$ MPa has the lowest continental difference, d_c^*, namely 1.85%. The first panel of Figure 5 displays magmatic periods, with distinctly visible, inactive periods between them. Expectedly, the maxima decrease as a function of time. This is a consequence of the decrease of the radiogenic heating of the mantle and of the general cooling of the Earth (cf. Figure 5, fourth panel). Models of a rapid generation of the whole CC *exclusively* in the Hadean and the Early Archean [*Armstrong*, 1981, 1991] are in contradiction to our model. *Hurley and Rand* [1969] concluded from whole-rock Rb-Sr isotopic compositions of CC that the main increase of CC was in the latest 1500 Ma and that there were nearly no CC additions in the Archean. This also conflicts with our results. Because of the cooling history of the Earth and because of the decrease of radiogenic energy, their model is extremely improbable. On the basis of investigations of greenstones and for other reasons, *O'Nions et al.* [1979], *Allègre* [1982], and *McCulloch and Bennett* [1994] derived a gradual increase of total continental mass over the whole Earth's history that is somewhat more related to our results. However, we also observe a CC contribution at the very beginning. With respect to the episodic segmentation of the contributions to the CC growth, the conclusions of *McCulloch and Bennett* [1994], *Stein and Hofmann* [1994], and *Condie* [1998] are similar to ours. The underestimation of the very early contribution is corrected in *Condie* [2000], considerably better rectified in *Condie and Aster* [2010]. The observed main maxima at ages of 2686, 1871, 1073, and 576 Ma according to the zircon dates by *Condie and Aster* [2010] are to be found fairly exactly at these points of time in the first panel of Figure 5 of our model. Admittedly, we found two further maxima in between. If we complement *Condie and Aster's* [2010] data by the ages of detrital zircons from sandstones and metasandstones of Figure 16 by *Bradley* [2011], then we find frequency peaks at 2697, 1824, *1435*, 1047, 594, *432*, and *174* Ma. These numbers confirm not only the four main maxima by *Condie and Aster* [2010] but also our additional peak near 1435 Ma. The large amplitude of the two latest maxima of *Bradley* [2011] is probably the result of preservation bias. Furthermore, *Bradley* [2011] points to the fact that the Neoarchean continental assembly of Superia broke

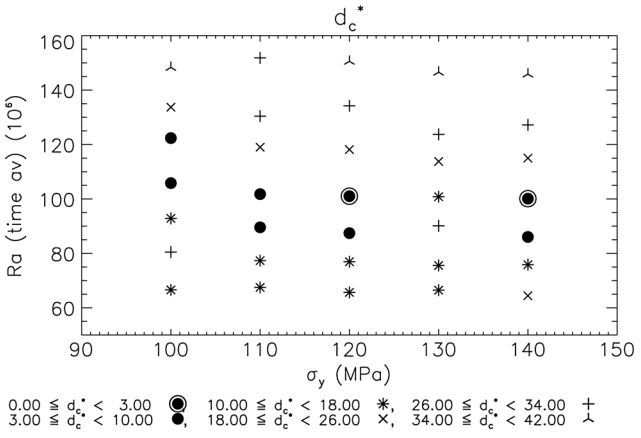

Figure 4. A comparison of several runs which differ only in the viscoplastic yield stress, σ_y, and the time average of the Rayleigh number, Ra, averaged between $\tau = 4490$ Ma and $\tau = 0$ Ma. The symbols represent the absolute value of the difference, d_c^*, between computed and observed present-day percentage of continents, expressed in percent.

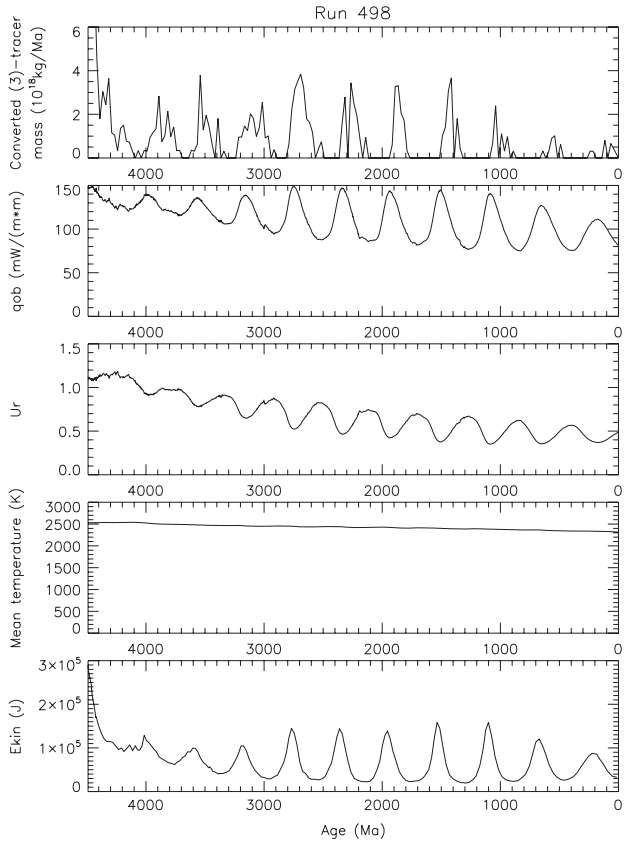

Figure 5. Curves showing the *evolution* for run 498 that is in best accordance with the observed continental surface percentage. The first panel shows the episodes of juvenile magmatic activity, the second one the laterally averaged heat flow density at the Earth's surface, and the third one the Urey number, *Ur*. The fourth panel presents the volumetrically averaged temperature of the mantle, T_{mean}, as a function of age. The fifth panel shows the kinetic energy of the solid-state creep convection in the mantle, E_{kin}.

up at about 2300 Ma. This corresponds to our last missing maximum younger than 2700 Ma. Figure 10 shows that the times of chemical differentiation events in our model are almost independent of the melting-criterion parameter f_3 of equation (9). This is remarkable because there are undoubtedly stochastic parts of the differentiated mass [*Walzer and Hendel*, 2009]. Figure 10 shows that the correspondence in the ages of theoretical and observed peaks is not by chance.

[23] For the parameters of run 498 and an age of τ = 2602.3 Ma, our model predicts an integrated tracer mass of 69.58% of the present-day mass of continents whereas, according to *Condie and Aster* [2010, Figure 9], the observed continental mass for τ = 2600 Ma is about 60% of the present-day mass. According to *Hawkesworth et al.* [2010] and *Belousova et al.* [2010], there was 70% of present-day volume of CC for an age of 2500 Ma. So it is evident that our model yields the right order of magnitude. In the face of the simplicity of our model, this is an acceptable result. It has been proposed that the isotopic ages of the continents are reflective of episodic magmatic events [*McCulloch and Bennett*, 1994; *Condie*, 1998]. At the same time, it is obvious that not only the generation, but also the preservation of CC, plays a role.

[24] Because of the good agreement of the numerical results of run 498 with observations, we now keep r_n and σ_y constant: r_n = 0.5 (which corresponds to $Ra \approx 10^8$) and σ_y = 120 MPa. Further variations of the parameters refer to the factor f_3 of equation (9), and to the thermal conductivity, k, keeping r_n and σ_y fixed at the mentioned two values. At a first glance on Figure 6, we could have the impression that there is a tradeoff between k and f_3 since optimal solutions (black circles with an outer ring) cluster along a certain curve. However, all other observable quantities in other f_3-k plots show that only the three optimum solutions with k = 5.0 W/(m K) in the upper right-hand corner of Figure 6 are realistic. Figure 7a demonstrates, e.g., that only thermal-conductivity values around k = 5.0 W/(m K) lead to solutions that are satisfactory for *all* observables, also for p_c of Figure 6. Also from the physical point of view, his value is acceptable [*Yoneda et al.*, 2009]. Therefore, we varied f_3 in small steps from 1.0 downward, keeping k = 5.0 W/(m K) constant. As expected from Figures 6 and 7a and similar f_3-k plots, we obtained very realistic solutions down to f_3 = 0.985. However, already f_3 = 0.983 and f_3 = 0.981 generate less convincing results.

[25] Figure 5 shows that the temporal variations of the laterally averaged heat flow, *qob* (second panel), the Urey number, *Ur* (third panel), and the kinetic energy of the convective creep, *Ekin* (fifth panel) contain a periodic superposition so that 900 Ma includes about two periods. Also in all other runs, we observe this fact. Therefore, we take the mean over the last 900 Ma of the Earth's history and obtain qob_9, Ur_9, $Ekin_9$ etc. to draw general comparisons. In accordance with *Gurnis and Davies* [1986] we find, however, that T_{mean} does *not* show essential temporal fluctuations, but decreases only very sluggishly and much less than predicted by parameterized Earth evolution models. For run 498, e.g., we find

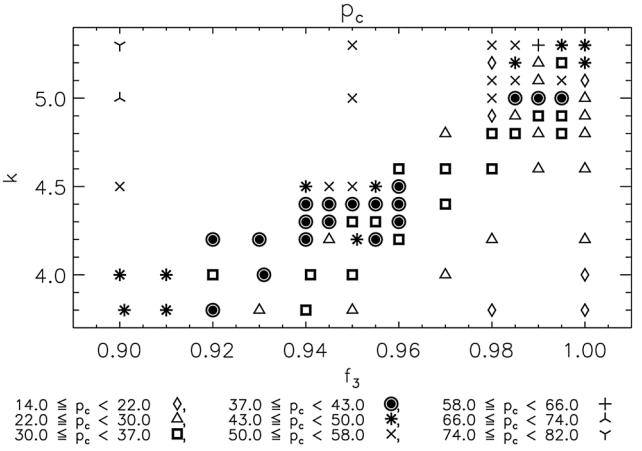

Figure 6. Keeping r_n = 0.5 and σ_y = 120 MPa fixed, the melting-criterion factor, f_3, and the thermal conductivity, k, are varied. The symbols represent intervals of the theoretical present-day continental surface, p_c, in percent. Note for comparison that 40.35% of the real present-day Earth is covered by continents and epicontinental seas. The optimal run, shown in Figure 5, corresponds to k = 5.0 W/(m K) and f_3 = 0.995.

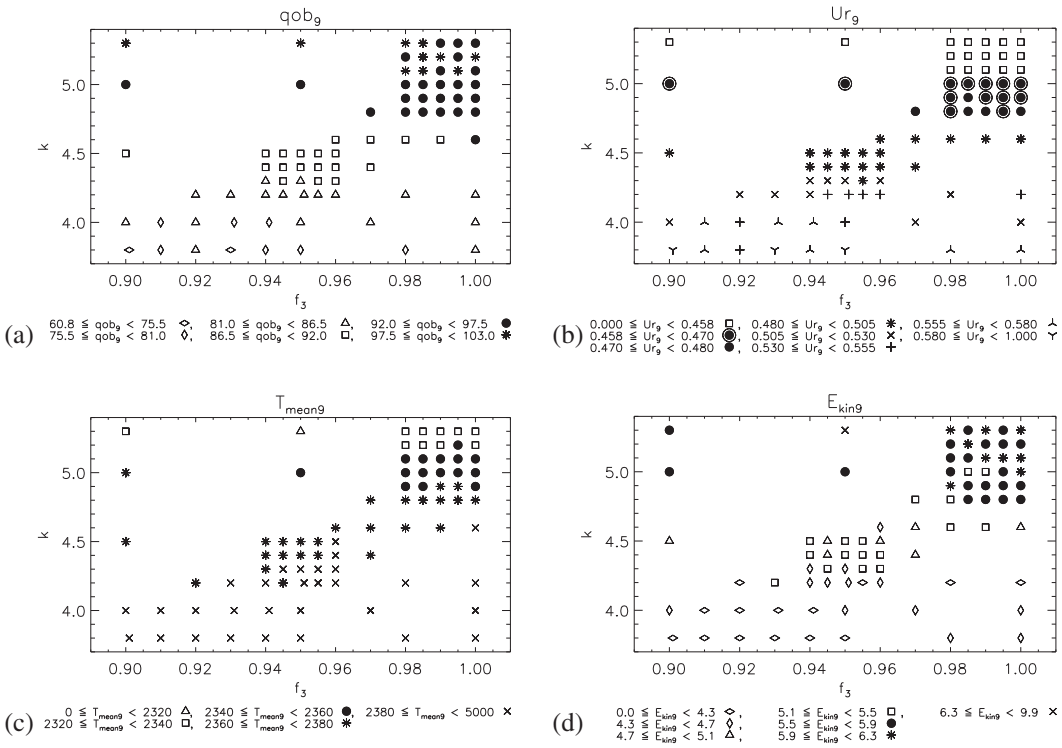

Figure 7. Four f_3-k plots for constant $r_n = 0.5$ and $\sigma_y = 120$ MPa. (a) The laterally averaged surface heat flow is *qob*. The temporal average of *qob* over the last 900 Ma is qob_9, in mW/m^2. (b) Ur_9 is the Urey number, *Ur*, averaged over the last 900 Ma. The most probable values of Ur_9 are denoted by black circles with a ring around them. (c) T_{mean} is the volumetrically averaged temperature in K. T_{mean9} is the temporal average of T_{mean} over the last 900 Ma. The most probable T_{mean9} values are depicted by black circles. (d) The kinetic energy of the creep, E_{kin9}, averaged over the last 900 Ma, in 10^4 J. The most probable E_{kin9} values are denoted by black circles.

$T_{\mathrm{mean}} = 2530.9$ K at $\tau = 4490$ Ma and $T_{\mathrm{mean}} = 2316.1$ K at $\tau = 0$ (Figure 5, fourth panel). While older models predict a significantly hotter Archean mantle [*Nisbet and Fowler*, 1983; *Abbott et al.*, 1994], younger models [e.g., *Grove and Parman*, 2004] suggest a wet, only slightly hotter Archean mantle. *Van Hunen et al.* [2008] conclude that the Archean mantle was only 100–300 K hotter than the present-day mantle, which is in good agreement with our results (Figure 5, fourth panel). From this it follows, in accordance with *Gurnis and Davies* [1986], that we can abandon the idea of *mantle wide, simultaneous* sets of thermal or chemical overturns that alter the overall thermal structure of the mantle relatively rapidly.

[26] Figure 8 shows rather realistic present-day distributions of continents (red) for the row of appropriate solutions in the upper right-hand corner of Figure 6 at $k = 5.0$ W/(m K).

[27] The Urey number, *Ur*, is the ratio of current total radiogenic heat generation to current heat output. The present-day Urey number, Ur_0, is not well constrained. *Christensen* [1985] concluded that Ur_0 is 0.5 or slightly less. *Jaupart et al.* [2007] combined estimations on surface heat flow measurements and geochemical estimations on the mantle's heat production and found values between 0.21 and 0.49. Numerical simulations by *Nakagawa and Tackley* [2012] result in $Ur_0 = 0.3$ to 0.5. Somewhat deviant from it, *Korenaga* [2008] deduced that the bulk Earth Urey ratio is about 0.35. By combination with other probably appropriate results of our model, we conclude that the most likely average value of *Ur* for the latest 900 Ma is within the interval $0.458 \leq Ur_9 < 0.470$ (see Figure 7b). For run 498, the special value Ur_0 is at 0.4885 but, of course, the averaged values Ur_9 are more relevant.

[28] Figure 7c shows a f_3-k plot of T_{mean9}. Runs with computed values near the corresponding observational values show a T_{mean9} between 2340 and 2360 K. Taking into account the strong increase of the geotherm immediately above the CMB, this interval is in agreement with the present-day T_{mean} value, called T_{mean0}, which can be estimated from results by *Katsura et al.* [2010]. Our T_{mean9} is only slightly higher than the T_{mean0} that can be computed from the results by *Stixrude et al.* [2009]. Whereas T_{mean} of all runs diminishes only slightly and nearly monotonously, the kinetic energy, E_{kin}, of the solid-state creep of mantle convection slowly oscillates in such a way that a temporal averaging over the latest 900 Ma makes sense. In this way, E_{kin9} was calculated and represented by the f_3-k plot of Figure 7d. The f_3-k plots of qob_9, Ur_9, T_{mean9}, and E_{kin9} in Figure 7 clearly show that the most appropriate values are close to $k = 5.0$ W/(m K) where appropriate refers to nearby observational or otherwise derived values. Because of the seeming tradeoff curve of the calculated present-day continental surface percentage, p_c, in the f_3-k plot (cf. Figure 6) and by comparison with the other f_3-k plots, it is evident that only the upper right-

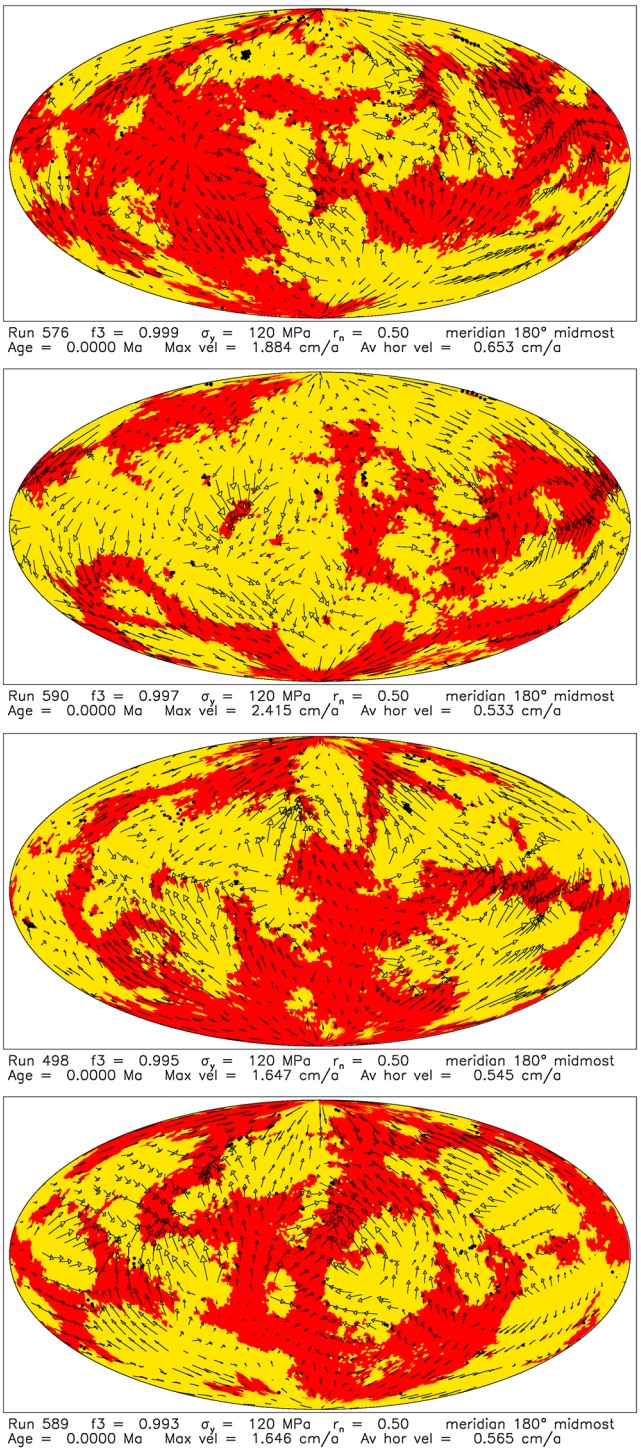

Figure 8. Present-day distribution of continents (red), oceanic lithosphere (yellow), and oceanic plateaus (black dots). r_n = 0.5, σ_y = 120 MPa, and k = 5.0 W/(m K) are kept constant. From top to bottom, we have f_3 = 0.999, f_3 = 0.997, f_3 = 0.995, and f_3 = 0.993, where the third panel (f_3 = 0.995) corresponds to run 498 shown in Figure 5. The arrows denote the present-day creep velocities at the surface.

hand square of the f_3-k plots and especially solutions close to k = 5.0 W/(m K) yield results which fulfill all requirements at the same time.

[29] Similar to the second panel of Figure 5, there is, for every other run, such a picture of slow oscillations, superimposed on a slight decrease of the laterally averaged surface heat flow, *qob*, as a function of time. The maxima of *qob* are always somewhat earlier than the assigned maxima of magmatic activity (cf. Figure 5, first panel). The present-day value of *qob*, called qob_0, always depends on the phases of the sinusoidal components of *qob*. Therefore, qob_9 is more significant than qob_0. For comparison we have, however, only qob_0 which is derived from surface measurements using different procedures of lateral averaging. Often qob_0 is somewhat smaller than qob_9, since there is a decreasing component in *qob*. *Pollack et al.* [1993] determined the observed present-day *total* heat flow, q_{to} = (44.2 ± 1) TW. This corresponds to a laterally averaged heat flow (density) of qob_0 = (86.7 ± 2) mW/m^2. *Jaupart et al.* [2007] made alternative interpretations of the same heat flow data set and arrived at q_{to} = (46 ± 3) TW which corresponds to qob_0 = (90 ± 6) mW/m^2. *Davies and Davies* [2010] used 38,347 heat flow measurements, accounted for hydrothermal circulation in young oceanic crust, averaged separately in the different geological units and estimated a total heat flow of q_{to} = (47 ± 2) TW corresponding to qob_0 = (92 ± 4) mW/m^2. Since qob_9 should somewhat exceed that value, we consider solutions with 92.0 mW/m^2 ≤ qob_9 < 97.5 mW/m^2 as appropriate and denote them by black circles in Figure 9a. The central run with r_n = 0.5 (corresponding to $Ra \approx 10^8$) and σ_y = 120 MPa belongs to that category of possible solutions.

[30] Figure 9b displays that our preferred, over 900 Ma averaged Urey number class, 0.458 ≤ Ur_9 < 0.47, does not very strongly depend on the temporally averaged Rayleigh number, *Ra*, but very well on the viscoplastic yield stress, σ_y. The most favorable solutions are on the line σ_y = 120 MPa. In contrast to Ur_9, the quantity T_{mean9} shows only a weak dependence on σ_y. It mainly depends on *Ra* (Figure 9c). This is easily understandable because the Rayleigh number is the ratio of buoyancy and viscous frictional forces. The thermal state of the *whole* mantle mainly depends on *Ra*. The heat emission at the *surface*, however, heavily depends on the structure of lithospheric plates. In the extreme case of a one-plate planet, the radiant emittance into space is minimal. The yield stress, however, in connection with the existence of the asthenosphere, enables an augmented surface heat flow. Because the usual Urey number is the mantle's heat generation divided by the surface heat loss at the same time, it is easily understandable that Ur_9 mainly depends on σ_y (cf. Figure 9b).

[31] Figure 9d shows that E_{kin9} depends on both, *Ra* and σ_y. This is qualitatively understandable from Figure 3. Because of the high viscosity in the middle part of the lower mantle, a large part of the mantle's kinetic energy is concentrated in the upper 1250 km. Therefore, the influence of σ_y (and of the lithospheric plates) on E_{kin9} is somewhat greater than on T_{mean9}. On these grounds, the chemical intermixture of the widespread distributed, modern chemical reservoirs is more intensive in the upper 1250 km of the mantle than in the main part of the lower mantle. Hence, a chance of survival of old, relatively little changed chemical reservoirs is maximal in the middle part of the lower mantle.

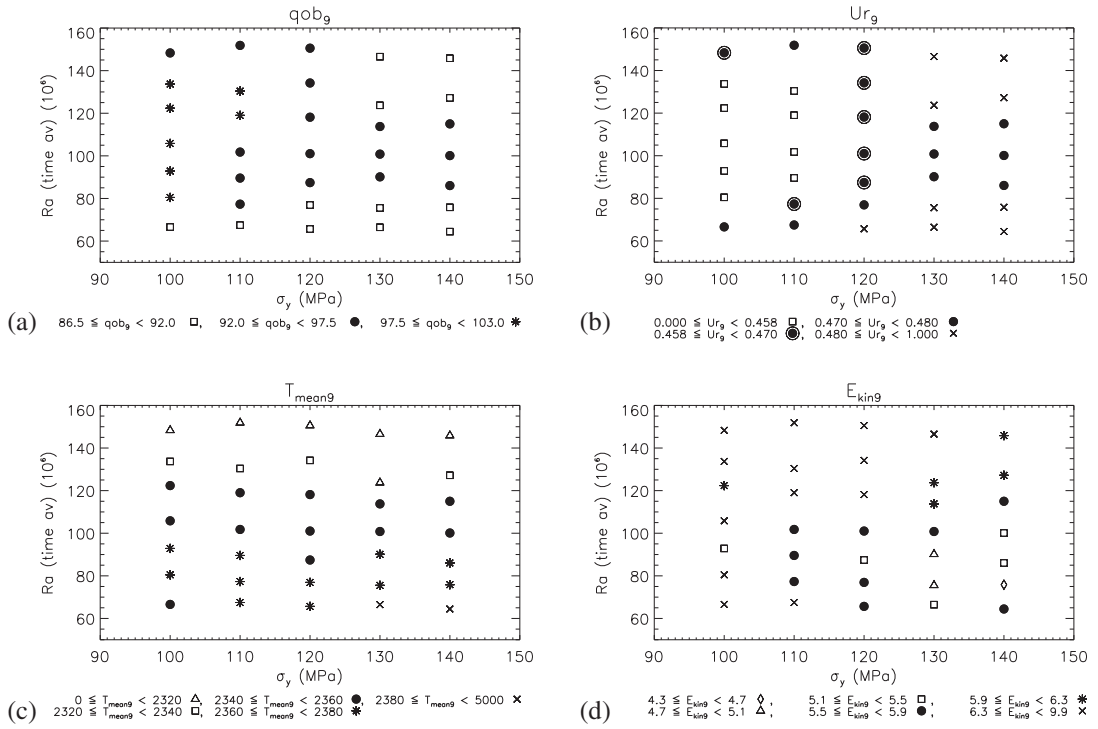

Figure 9. Four $\sigma_y - Ra$ plots for f_3 = 0.995, and k = 5.0 W/(m K). (a) qob_9 in mW/m^2. Black dots denote realistic qob_9. (b) The Urey number, Ur_9, averaged over the last 900 Ma. (c) T_{mean9} in K. (d) E_{kin9} in 10^4 J. For further explanation, cf. Figure 7.

Also the low lateral movability of CMB-based plumes can be explained by this highly viscous central part of the lower mantle.

4. Discussion

[32] In our model, we assume that the essential features of the mechanism of Archean plate tectonics only quantitatively differ from present-day plate tectonics. This assumption is corroborated by *Komiya et al.* [1999], who have shown that the origin of plate tectonics dates back to at least 3.8 Ga. *Komiya* [2004] proved the MORB affinity of samples from five different-aged Archean sandstone belts. Early Archean greenstone belts resemble circum-Pacific accretionary complexes in the Phanerozoic. That proves that the concept of accretionary geology is also applicable to the Archean. Furthermore, 4.4–4.0 Ga zircons have a chemical and isotopic signature suggesting derivation from the felsic melts of the TTG suite that suggests the occurrence of plate tectonics back to 4.4 Ga [*Iizuka et al.*, 2010; *Maruyama et al.*, 2013].

[33] Our results confirm the observation that the geological evolution is not continuous. In accordance with *Komiya* [2011], we assert that continental growth is determined by both efflux from the mantle and recycling of CC material back into the mantle. The corresponding tracer method is described in *Walzer and Hendel* [2008]. The results of our numerical model also show quiescent intervals of magmatic evolution (Figure 10) in agreement with observation. The geochemical development of the earliest Archean reveals early sudden continental growth [*McCulloch and Bennett*, 1994]. Obviously, there are diverse mechanisms that contribute to the production of CC. The occurrence of komatiites in the late Archean and ocean-island-basalt-type magmatism in the early Proterozoic [*Stern et al.*, 1995; *Abbott et al.*, 1997] corroborates the opinion that in this early time, plume-related volcanism contributed more to a preliminary stage of CC generation than at present. However, the Archean CC is dominated by TTG compositions. Some Archean TTGs are directly derived by slab melting, and others are mixtures of slab magmas and older CC [*Rollinson*, 2006]. Obviously, the subducted oceanic crust was partially molten to generate the Archean TTG. The extraction of TTG melts produced a dense garnet-bearing phase that foundered down to the mantle [*Hayashi et al.*, 2000; *Komiya et al.*, 2002; *Rino et al.*, 2004]. The most significant geochemical bulk CC models are andesitic [*Rudnick and Gao*, 2003; *McLennan et al.*, 2006]. Therefore, any basaltic composition, e.g., the high-Mg basalt compositions of Phanerozoic arcs, is not directly appropriate [*Kelemen et al.*, 2003]. Hence, an additional fractionation of the crust is needed, e.g., Model 5 by *Davidson and Arculus* [2006] or another mechanism of lower crustal and mantle-lithospheric foundering [*Kay and Mahlburg-Kay*, 1991] who expressed the idea that an olivine-, pyroxene-, and garnet-rich residue sinks into the mantle. *Hacker et al.* [2011] investigated the idea that the mantle generates differentiated crust in intra-oceanic arcs. They inferred that the middle and lower CC together contain large volumes of felsic crust that is positively buoyant and that can relaminate the base of the upper CC. The mentioned mechanisms are *not* mutually exclusive but might complement each other.

[34] *Rino et al.* [2004] and *Komiya* [2011] describe different categories of CC growth models: Parameterized forward

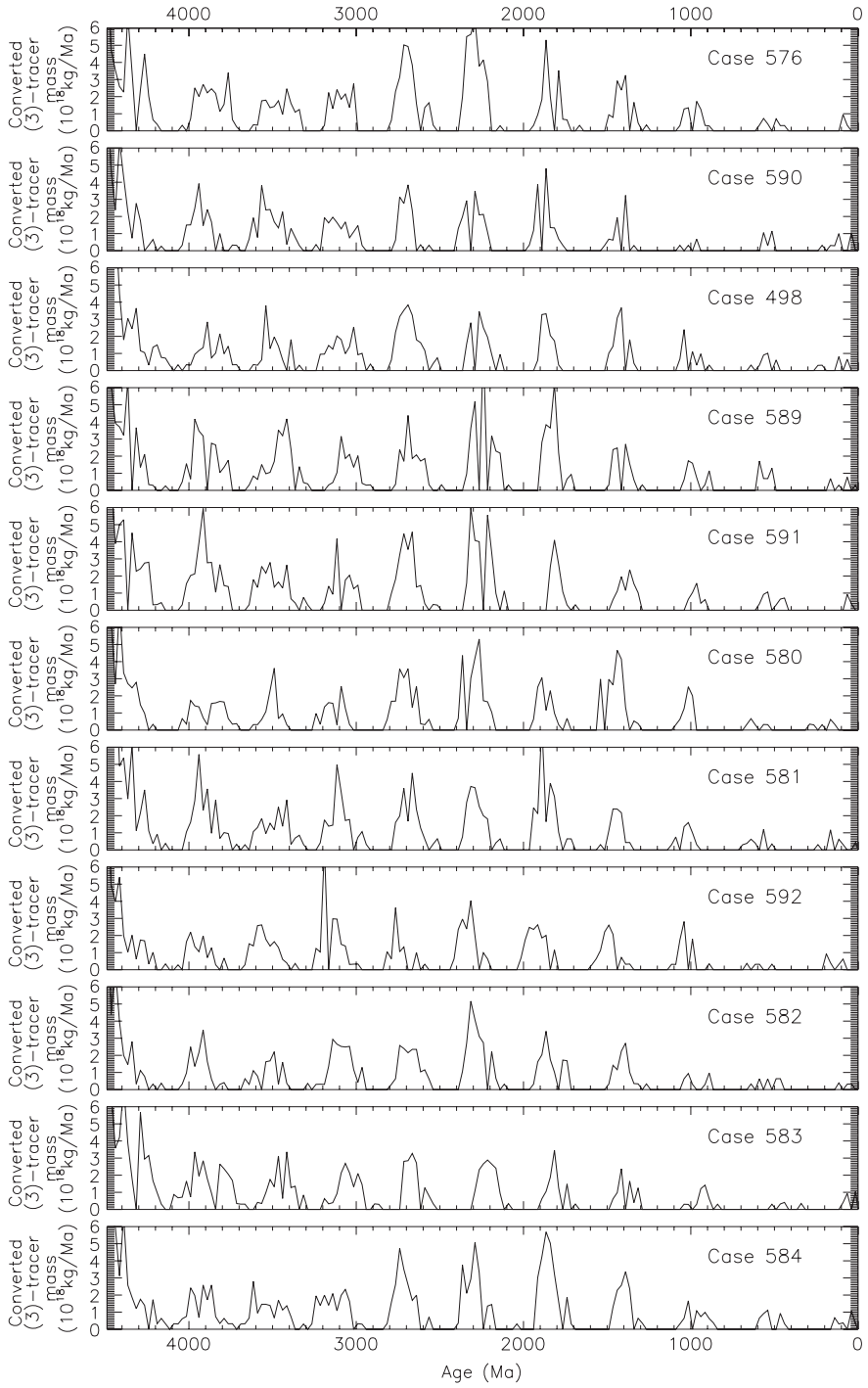

Figure 10. The distributions of the episodes of juvenile magmatic activity that contributed to the continental growth as a function of age. We varied the melting-criterion parameter, f_3, from (top panel) 0.999 to (bottom panel) 0.979 in steps of 0.002. The quantities σ_y = 120 MPa, r_n = 0.5, and k = 5.0 W/(m K) are kept constant.

models of thermal mantle evolution imply rapid growth. Geochemical estimates lead to moderate growth. The distribution of the still conserved CC results in slow growth. It is evident that recycling of CC plays a role. Here, we account for it only by a simplified procedure [*Walzer and Hendel*, 2008] and other publications (cf. http://www.igw.uni-jena.de/geodyn). Many other authors describe basically conceptual models where only specific parts of it are based on physics or isotope systematics. We solve, however, a closed system using the full set of balance equations. It is evident that each type of model has assets and drawbacks.

[35] Formerly, the difference between the potential temperatures of the Archean upper mantle and the present-time upper mantle was put at about 600 K [*Takahashi*, 1990;

Nisbet et al., 1993]. These estimates were corroborated by parameterized Earth evolution calculations. Today, it is generally accepted that komatiites do *not* represent the normal Archean mantle but correspond to upwelling diapirs or plumes. Already *Hayashi et al.* [2000] estimated that the temperature of Archean subducting slabs was only 200 K higher than that of Phanerozoic slabs. A comparison of *Komiya* [2011, Figure 7] and our run 498 for the upper mantle temperature drop during the last 3.8 Ga results in about 150 K and 142 K, respectively. Therefore, we conclude that the mantle's cooling down is not so large as thought before.

5. Synthesis

[36] Now we want to give a condensed answer to the question asked in the title of this paper. *Hawkesworth et al.* [2009] concluded that the frequency peaks of the zircon crustal age estimates reflect differences in the preservation potential of CC rather than episodic phases of elevated CC-generation. *Belousova et al.* [2010] hold the same view and add the opinion that "modeling suggests that there was little episodicity in the production of new crust, as opposed to peaks in magmatic ages." By means of our model, we show first that the reality is probably between their proposal and episodic growth of continents and second that our physically grounded, dynamic modeling results in episodic augmentation events of juvenile CC. With only a few constraints, our model also yields a lot of other geophysical results that are close to observations. The preservation potential is *also* connected with the convection-differentiation mechanism of the mantle via supercontinents.

[37] Many models are preferably conceptual and do not have a broad physical background. In some of the mechanisms of other authors who have been discussed in section 1.2, some aspect is chosen to be the center, e.g., plates or plumes. In the present model, however, plates and plumes develop self-consistently. Furthermore, we do not simply put the continents on the surface but they develop from the convection-differentiation system. We prescribe neither the number of continents nor their form and size, nor their angular velocity from which the drift velocity at the surface can be computed. The time dependence of angular velocity of continents, location, time, and speed of the chemical differentiation of the mantle and the accretion of the differentiation products to a continent developed from the system of equations and are also not prescribed. Many models, however, try to answer a *singular* question as, e.g., the question of our title, and touch the other observations only casually. We think that a numerical model that solves *several* problems *simultaneously* is a better approach to geological reality.

[38] *The most important features of the present model*. We solve the conservation equations of mass, momentum, energy, and angular momentum. The mechanism of chemical differentiation is formulated in such a way that the four sums of the number of atoms of the pairs ^{238}U-^{206}Pb, ^{235}U-^{207}Pb, ^{232}Th-^{208}Pb, and ^{40}K-^{40}Ar are conserved, too. The present model is not only a box and flux model. The viscosity is pressure and temperature dependent. It is supplemented by a viscoplastic yield stress, σ_y. We introduced a new viscosity function, η_4, the upper mantle of which is characterized by a first low viscosity layer. This conventional asthenosphere and σ_y are the essential prerequisites for the piecewise plate-like behavior of the lithosphere near the surface. It is essential that also the oceanic lithosphere develop exclusively not only by the temperature dependency of the viscosity but also by a chemical difference between the oceanic lithosphere and the rest of the mantle [*Rychert and Shearer*, 2009]. If this would not be the case, then we would be unable to explain the sharp viscosity jump at the lithosphere-asthenosphere boundary. Up to now, for numerical reasons, we could not incorporate that viscosity jump but replaced it by a steep gradient. The used solidus curves are relevant for the condition of chemical differentiation. The solidus depends not only on pressure but also on water abundance. Because of the latter dependence, we obtained a time-dependent solidus for the upper 660 km of the mantle. We deduced a new extended acoustic Grüneisen parameter, γ_{ax}, by means of which we could determine a realistic adiabatic temperature profile.

[39] *The most relevant dynamic results.* We intensively investigated the space of the parameters Ra, σ_y, f_3 and k and solved the system of equations at every examined point for the latest 4490 Ma of the Earth's evolution where the mantle is represented by 1,351,746 nodes in an icosahedral grid and 10,486,272 tracer particles. Stability test cases ran with 10,649,730 grid points and 83,887,104 tracer particles. The essential idea was that for *all* investigated questions, the simulation should simultaneously produce acceptable results. Solutions with Ra at about 10^8 produce good approximations of the observed present-day mass of the continents. The quantity, d_c^*, appropriate for it, only little depends on σ_y. The same applies for T_{mean9}. However, Ur_9 mainly depends on σ_y and less on Ra. The majority of the most appropriate values are to be found at the line of σ_y = 120 MPa. The quantity E_{kin9} depends on both Ra and σ_y.

[40] Figure 7 shows related distributions of qob_9, Ur_9, T_{mean9}, and E_{kin9} of the most appropriate cases in the f_3-k plot. These plots strongly differ from the f_3-k plot of the deviation of the calculated continental size from the observed one, p_c, in Figure 6. By comparison, one can find a *common* set of appropriate cases in the upper right-hand corners which show the best agreement for k = 5.0 W/(m K). Therefore, we finally vary only the melting-criterion parameter, f_3. As a result, we obtain a set of temporal distributions of *continental crustal growth episodes* that show a certain temporal invariance in spite of the variation of f_3. These episodes are distinctly separated by time intervals of magmatic quiescence. It is remarkable that also the other results of these cases are in agreement with observations. Figure 5 shows the *general mantle evolution* that is likewise acceptable. *Condie and Aster's* [2010] and *Bradley's* [2011] zircon and sandstone age estimates result in *peaks of frequency* at 2697, 1824, *1435*, 1047, 594, *432*, and *174* Ma that are reproduced by run 498 (cf. Figures 5 and 10). This statement implies by no means that the preservation potential does not play a role. It is, however, evident that *a physically based modeling indicates that it is possible to reproduce essential parts of the episodicity in the production of new continental crust and that this episodicity is temporally associated with the zircon age data.*

[41] Although qob, Ur, and E_{kin} distinctly show temporally sinusoidal components, the physics of mantle

convection reveals that the volumetrically averaged mantle temperature, T_{mean}, *does not change rapidly and is monotonously decreasing*. This statement corroborates a principal result of *Gurnis and Davies* [1986]. The present model shows a slow decay of T_{mean} by about 215 K over the last 4490 Ma. This result is compatible with observations (cf. section 4). For the mechanism of episodic juvenile growth of continents *with quiet time intervals*, it seems to be important that the upper mantle solidus is dependent not only on pressure but also on the *water abundance*. We emphasize that the episodic partial melting and differentiation events result immediately from the system of mantle convection theory plus mantle cooling plus water-abundance dependence of the solidus. The spatial mantle distribution of the depleted MORB mantle and the reservoirs that are richer in incompatible elements is like a marble cake and without sharp boundaries.

[42] Finally, we remark that especially the amplitudes of the younger magmatic episodes (cf. Figure 10) decrease considerably. This is to be expected because of the secular cooling of the Earth and due to decreasing radiogenic heat production. Also in all other computational cases, not shown here, we find this decrease and the episodicity of the growth of continental mass. We do not exclude the possible influence of the preservation potential on the distribution of zircon crustal age estimates particularly because this potential is indirectly also determined by mantle convection. One of our principal findings is that genuine dynamic modeling results in a pronounced episodicity of chemical differentiation. The differentiation products are collected in terranes that are episodically accreted to a continent. The temporal sequence of magmatic episodes is in reasonable agreement with the observed peaks of zircon crustal age estimates. This is noteworthy because the chosen physical parameters accord with the general geophysical consensus.

[43] **Acknowledgments.** We gratefully acknowledge the stimulating discussions with J. Baumgardner, H.-P. Bunge, P. Bollada, H. Davies, R. Davies, C. Köstler, M. Mohr, and M. Müller in the group of Terra developers. This work benefited from geological and geochemical discussions with J. Kley and L. Viereck-Götte. We thank T. Parsons, P. Benson, T. Komiya, J. Geissman, and an anonymous reviewer for editing, reviewing, and helping to improve the initial manuscript. We acknowledge the Steinbuch Center for Computing, Karlsruhe, for the supply of computational time under grant sphshell. This work was partly supported by the Deutsche Forschungsgemeinschaft under grant KL 495/16-1.

References

Abbott, D., R. Drury, and W. H. F. Smith (1994), Flat to steep transition in subduction style, *Geology*, *22*, 937–940.

Abbott, D. H., R. Drury, and W. D. Mooney (1997), Continents as lithological icebergs: The importance of buoyant lithospheric roots, *Earth Planet. Sci. Lett.*, *149*, 15–27.

Albarède, F. (1998), The growth of continental crust, *Tectonophysics*, *296*, 1–14.

Allègre, C. J. (1982), Chemical geodynamics, *Tectonophysics*, *81*, 109–132

Anderson, O. L. (1995), *Equations of State of Solids for Geophysics and Ceramic Science*, 405 pp., Oxford Univ. Press, New York.

Armstrong, R. L. (1981), Radiogenic isotopes: The case for crustal recycling on a near-steady-state no-continental-growth Earth, *Phil. Trans. R. Soc. Lond. A*, *301*, 443–472.

Armstrong, R. L. (1991), The persistent myth of crustal growth, *Austral. J. Earth Sci.*, *38*, 613–630.

Belousova, E. A., Y. A. Kostitsyn, W. L. Griffin, G. C. Begg, S. Y. O'Reilly, and N. J. Pearson (2010), The growth of the continental crust: Constraints from zircon Hf-isotope data, *Lithos*, *119*, 457–466, doi:10.1016/j.lithos.2010.07.024.

Blichert-Toft, J., and F. Albarède (2008), Hafnium isotopes in Jack Hills zircons and the formation of the Hadean crust, *Earth Planet. Sci. Lett.*, *265*, 686–702, doi:10.1016/j.epsl.2007.10.054.

Boyet, M., and R. W. Carlson (2006), A new geochemical model for the Earth's mantle inferred from ^{146}Sm–^{142}Nd systematics, *Earth Planet. Sci. Lett.*, *250*, 254–268, doi:10.1016/j.epsl.2006.07.046.

Bradley, D. (2011), Secular trends in the geologic record and the supercontinent cycle, *Earth-Science Rev.*, *108*, 16–33, doi:10.1016/j.earscirev.2011.05.003.

Caro, G. (2011), Early silicate Earth differentiation, *Annu. Rev. Earth Planet. Sci.*, *39*, 31–58, doi:10.1146/annurev-earth-040610-133400.

Christensen, U. R. (1985), Thermal evolution models for the Earth, *J. Geophys. Res.*, *90*, 2995–3007.

Christensen, U. R., and D. A. Yuen (1985), Layered convection induced by phase transitions, *J. Geophys. Res.*, *90*, 10,291–10,300.

Clift, P. D., P. Vannucchi, and J. Phipps Morgan (2009), Crustal redistribution, crust-mantle recycling and Phanerozoic evolution of the continental crust, *Earth-Science Rev.*, *97*, 80–104, doi:10.1016/earscirev.2009.10.003.

Coffin, M. F., and O. Eldholm (1994), Large igneous provinces: Crustal structure, dimensions and external consequences, *Rev. Geophys.*, *32*, 1–36.

Condie, K. C. (1998), Episodic continental growth and supercontinents: A mantle avalanche connection? *Earth Planet. Sci. Lett.*, *163*, 97–108.

Condie, K. C. (2000), Episodic continental growth models: Afterthoughts and extensions, *Tectonophysics*, *322*, 153–162.

Condie, K. C., and R. C. Aster (2010), Episodic zircon age spectra of orogenic granitoids: The supercontinent connection and continental growth, *Precambr. Res.*, *180*, 227–236, doi:10.1016/j.precamres.2010.03.008.

Davidson, J. P., and R. J. Arculus (2006), The significance of Phanerozoic arc magmatism in generating continental crust, in *Evolution and Differentiation of the Continental Crust*, edited by M. Brown and T. Rushmer, pp. 135–172, Cambridge Univ. Press, Cambridge, UK.

Davies, G. F. (2007), Controls on density stratification in the early mantle, *Geochem. Geophys. Geosys.*, *8*, Q04,006, doi:10.1029/2006GC001414.

Davies, G. F. (2008), Episodic layering of the early mantle by the 'basalt barrier' mechanism, *Earth Planet. Sci. Lett.*, *275*, 382–392, doi:10.1016/j.epsl.2008.08.036.

Davies, J. H., and D. R. Davies (2010), Earth's surface heat flux, *Solid Earth*, *1*, 5–24.

Dziewonski, A. M., and D. L. Anderson (1981), Preliminary reference Earth model, *Phys. Earth Planet. Int.*, *25*, 297–356.

Grove, T. L., and S. W. Parman (2004), Thermal evolution of the Earth as recorded by komatiites, *Earth Planet. Sci. Lett.*, *219*, 173–187, doi:10.1016/S0012-821X(04)00002-0.

Guitreau, M., J. Blichert-Toft, H. Martin, S. J. Mojzsis, and F. Albarède (2012), Hafnium isotope evidence from Archean granitic rocks for deep-mantle origin of continental crust, *Earth Planet. Sci. Lett.*, *337*, 211–223, doi:10.1016/j.epsl.2012.05.029.

Gurnis, M., and G. F. Davies (1986), Apparent episodic crustal growth arising from a smoothly evolving mantle, *Geology*, *14*, 396–399.

Hacker, B. R., P. B. Kelemen, and M. D. Behn (2011), Differentiation of the continental crust by relamination, *Earth Planet. Sci. Lett.*, *307*, 501–516.

Harrison, T. M., J. Blichert-Toft, W. Müller, F. Albarède, P. Holden, and S. J. Mojzsis (2005), Heterogeneous Hadean hafnium: Evidence of continental crust at 4.4 to 4.5 Ga, *Science*, *310*, 1947–1950.

Harrison, T. M., A. K. Schmitt, M. T. McCulloch, and O. M. Lovera (2008), Early ($\geq$ 4.5 Ga) formation of terrestrial crust: Lu–Hf, δ^{18}O, and Ti thermometry results for Hadean zircons, *Earth Planet. Sci. Lett.*, *268*, 476–486.

Hawkesworth, C. J., and A. I. S. Kemp (2006), Using hafnium and oxygen isotopes in zircons to unravel the record of crustal evolution, *Chem. Geol.*, *226*, 144–162.

Hawkesworth, C. J., P. A. Cawood, A. I. S. Kemp, C. D. Storey, and B. Dhuime (2009), A matter of preservation, *Science*, *323*, 49–50.

Hawkesworth, C. J., B. Dhuime, A. B. Pietranik, P. A. Cawood, A. I. S. Kemp, and C. D. Storey (2010), The generation and evolution of the continental crust, *J. Geol. Soc. London*, *167*, 229–248.

Hayashi, M., T. Komiya, Y. Nakamura, and S. Maruyama (2000), Archean regional metamorphism of the Isua supracrustal belt, southern West Greenland: Implications for a driving force for Archean plate tectonics, *Int. Geol. Rev.*, *42*, 1055–1115.

Hofmann, A. W. (1988), Chemical differentiation of the Earth: The relationship between mantle, continental crust and oceanic crust, *Earth Planet. Sci. Lett.*, *90*, 297–314.

Hofmann, A. W. (1997), Mantle geochemistry: The message from oceanic volcanism, *Nature*, *385*, 219–229.

Hofmann, A. W. (2003), Sampling mantle heterogeneity through oceanic basalts: Isotopes and trace elements, in *Treatise on Geochemistry Vol.2:*

The Mantle and the Core, edited by R. W. Carlson, pp. 61–101, Elsevier, Amsterdam.

Hurley, P. M., and J. R. Rand (1969), Pre-drift continental nuclei, *Science*, *164*, 1229–1242.

Iizuka, T., K. Horie, T. Komiya, S. Maruyama, T. Hirata, H. Hidaka, and B. F. Windley (2006), 4.2 Ga zircon xenocryst in an Acasta gneiss from northwestern Canada: Evidence for early continental crust, *Geology*, *34*, 245–248.

Iizuka, T., M. T. McCulloch, T. Komiya, T. Shibuya, K. Ohta, H. Ozawa, E. Sugimura, and K. D. Collerson (2010), Monazite geochronology and geochemistry of meta-sediments in the Narryer Gneiss Complex, Western Australia: Constraints on the tectonothermal history and provenance, *Contrib. Mineral. Petrol.*, *160*, 803–823.

Jaupart, C., S. Labrosse, and J.-C. Mareschal (2007), Temperatures, heat and energy in the mantle of the Earth, in *Treatise on Geophysics, Vol. 7: Mantle Dynamics*, edited by D. Bercovici, pp. 253–303, Elsevier, Amsterdam.

Karato, S.-I. (2008), *Deformation of Earth Materials: An Introduction to the Rheology of Solid Earth*, 463 pp., Cambridge Univ. Press, Cambridge, UK.

Katsura, T., A. Yoneda, D. Yamazaki, T. Yoshino, and E. Ito (2010), Adiabatic temperature profile in the mantle, *Phys. Earth Planet. Int.*, *183*, 212–218.

Kay, R. W., and S. Mahlburg-Kay (1991), Creation and destruction of lower continental crust, *Geol. Rundsch.*, *80*, 259–278.

Kelemen, P. B., G. M. Yogodzinski, and D. W. Scholl (2003), Along-strike variation in the Aleutian island arc: Genesis of high Mg# andesite and implications for continental crust, in *Inside the Subduction Factory, Geophysical Monograph Series,* vol. 138, edited by J. Eiler, pp. 223–276, AGU, Washington, D.C., doi:10.1029/138GM11.

Komiya, T. (2004), Material circulation model including chemical differentiation within the mantle and secular variation of temperature and composition of the mantle, *Phys. Earth Planet. Int.*, *146*, 333–367.

Komiya, T. (2011), Continental recycling and true continental growth, *Russ. Geol. Geophys.*, *52*, 1516–1529.

Komiya, T., S. Maruyama, T. Masuda, S. Nohda, M. Hayashi, and K. Okamoto (1999), Plate tectonics at 3.8–3.7 Ga: Field evidence from the Isua accretionary complex, southern West Greenland, *J. Geol.*, *107* (5), 515–554.

Komiya, T., M. Hayashi, S. Maruyama, and H. Yurimoto (2002), Intermediate-P/T type Archean metamorphism of the Isua supracrustal belt: Implications for secular change of geothermal gradients at subduction zones and for Archean plate tectonics, *Am. J. Sci.*, *302*, 806–826.

Korenaga, J. (2008), Urey ratio and the structure and evolution of Earth's mantle, *Rev. Geophys.*, *46*, RG2007, 32 pp., doi: 10.1029/2007RG00241.

Litasov, K. D. (2011), Physicochemical conditions for melting in the Earth's mantle containing a C-O-H fluid (from experimental data), *Russian Geol. & Geophys.*, *52*, 475–492.

Maruyama, S., M. Ikoma, H. Genda, K. Hirose, T. Yokoyama, and M. Santosh (2013), The naked planet Earth: Most essential pre-requisite for the origin and evolution of life, *Geosci. Front.*, *4*, 141–165.

McCulloch, M. T., and V. C. Bennett (1993), Progressive growth of the Earth's continental crust and depleted mantle: Constraints from ^{143}Nd-^{142}Nd isotopic systematics, *Lithos*, *30*, 237–255.

McCulloch, M. T., and V. C. Bennett (1994), Progressive growth of the Earth's continental crust and depleted mantle: Geochemical constraints, *Geochim. Cosmochim. Acta*, *58*, 4717–4738.

McLennan, S. M., S. R. Taylor, and S. R. Hemming (2006), Composition, differentiation, and evolution of continental crust: Constraints from sedimentary rocks and heat flow, in *Evolution and Differentiation of the Continental Crust*, edited by M. Brown and T. Rushmer, pp. 92–134, Cambridge Univ. Press, Cambridge, UK.

Mierdel, K., H. Keppler, J. R. Smyth, and F. Langenhorst (2007), Water solubility in aluminous orthopyroxene and the origin of the Earth's asthenosphere, *Science*, *315*, 364–368, doi: 10.1126/science.1135422.

Mitrovica, J. X., and A. M. Forte (2004), A new inference of mantle viscosity based upon joint inversion of convection and glacial isostatic adjustment data, *Earth Planet. Sci. Lett.*, *225*(1), 177–189.

Nakagawa, T., and P. J. Tackley (2004), Thermo-chemical structure in the mantle arising from a three-component convective system and implications for geochemistry, *Phys. Earth Planet. Int.*, *146*, 125–138.

Nakagawa, T., and P. J. Tackley (2012), Influence of magmatism on mantle cooling, surface heat flow and Urey ratio, *Earth Planet. Sci. Lett.*, *329*, 1–10.

Nisbet, E. G., and C. M. R. Fowler (1983), Model for Archean plate tectonics, *Geology*, *11*, 376–379.

Nisbet, E. G., M. J. Cheadle, N. T. Arndt, and M. J. Bickle (1993), Constraining the potential temperature of the Archean mantle: A review of the evidence from komatiites, *Lithos*, *30*, 291–307.

Nolet, G., R. Allen, and D. Zhao (2007), Mantle plume tomography, *Chem. Geol.*, *241*, 248–263.

Ogawa, M. (2008), Mantle convection: A review, *Fluid Dyn. Res.*, *40*, 379–398, doi:10.1016/j.fluiddyn.2007.09.001.

O'Neill, C., A. Lenardic, L. Moresi, T. H. Torsvik, and C. T. A. Lee (2007), Episodic Precambrian subduction, *Earth Planet. Sci. Lett.*, *262*, 552–562.

O'Neill, C. J., A. Lenardic, W. L. Griffin, and S. Y. O'Reilly (2008), Dynamics of cratons in an evolving mantle, *Lithos*, *102*, 12–24.

O'Nions, R. K., N. M. Everson, and P. J. Hamilton (1979), Geochemical modeling of mantle differentiation and crustal growth, *J. Geophys. Res.*, *84*, 6091–6101.

Patchett, J. P., and N. T. Arndt (1986), Nd isotopes and tectonics of 1.9-1.7 Ga crustal genesis, *Earth Planet. Sci. Lett.*, *78*, 329–338.

Poirier, J. P. (2000), *Introduction to the Physics of the Earth's Interior*, 312 pp., Cambridge Univ. Press, Cambridge, UK.

Pollack, H. N., S. J. Hurter, and J. R. Johnson (1993), Heat flow from the Earth's interior: Analysis of the global data set, *Rev. Geophys.*, *31*, 267–280.

Richter, F. M. (1973), Finite amplitude convection through a phase boundary, *Geophys. J. R. Astron. Soc.*, *35*, 265–276.

Rino, S., T. Komiya, B. F. Windley, I. Katayama, A. Motoki, and T. Hirata (2004), Major episodic increases of continental crustal growth determined from zircon ages of river sands; implications for mantle overturns in the Early Precambrian, *Phys. Earth Planet. Int.*, *146*, 369–394.

Roberts, N. M. W. (2011), Increased loss of continental crust during supercontinent amalgamation, *Gondwana Res.*, doi:10.1016/j.gr.2011.08.001.

Rollinson, H. (2006), Crustal generation in the Archean, in *Evolution and Differentiation of the Continental Crust*, edited by M. Brown and T. Rushmer, pp. 173–230, Cambridge Univ. Press, Cambridge, UK.

Rudnick, R. L., and D. M. Fountain (1995), Nature and composition of the continental crust: A lower crustal perspective, *Rev. Geophys.*, *33*, 267–309.

Rudnick, R. L., and S. Gao (2003), Composition of the continental crust, in *Treatise on Geochemistry, Vol.3: The Crust*, edited by R. L. Rudnick, pp. 1–64, Elsevier, Amsterdam.

Rychert, C. A., and P. M. Shearer (2009), A global view of the lithosphere-asthenosphere boundary, *Science*, *324*, 495–498.

Schubert, G., D. L. Turcotte, and T. R. Olson (2001), *Mantle Convection in the Earth and Planets*, pp. 1–940, Cambridge Univ. Press, Cambridge, U.K.

Stacey, F. D., and P. M. Davis (2009), *Physics of the Earth*, 4th ed., pp. 1–521, Cambridge Univ. Press, Cambridge, U.K.

Stein, M., and A. W. Hofmann (1994), Mantle plumes and episodic crustal growth, *Nature*, *372*, 63–68.

Steinbach, V., D. A. Yuen, and W. L. Zhao (1993), Instabilities from phase transitions and the timescales of mantle thermal convection, *Geophys. Res. Lett.*, *20*, 1119–1122.

Stern, R. A., E. C. Syme, and S. B. Lucas (1995), Geochemistry of 1.9 Ga MORB-and OIB-like basalts from the Amisk collage, Flin Flon Belt, Canada: Evidence for an intra-oceanic origin, *Geochim. Cosmochim. Acta*, *59*, 3131–3154.

Stern, R. J., and D. W. Scholl (2010), Yin and yang of continental crust creation and destruction by plate tectonic processes, *Int. Geology Rev.*, *52*, 1–31, doi:10.1080/00206810903332322.

Stixrude, L., and C. Lithgow-Bertelloni (2007), Influence of phase transformations on lateral heterogeneity and dynamics in Earth's mantle, *Earth Planet. Sci. Lett.*, *263*, 45–55.

Stixrude, L., and C. Lithgow-Bertelloni (2010), Thermodynamics of the Earth's mantle, *Rev. Min. Geochem.*, *71*, 465–484.

Stixrude, L., N. de Koker, N. Sun, M. Mookherjee, and B. B. Karki (2009), Thermodynamics of silicate liquids in the deep Earth, *Earth Planet. Sci. Lett.*, *278*, 226–232.

Stracke, A., A. W. Hofmann, and S. R. Hart (2005), FOZO, HIMU and the rest of the mantle zoo, *Geochem. Geophys. Geosys.*, *6*, Q05,007, doi: 10.1029/2004GC000824.

Stracke, A., J. E. Snow, E. Hellebrand, A. von der Handt, B. Bourdon, K. Birbaum, and D. Günther (2011), Abyssal peridotite Hf isotopes identify extreme mantle depletion, *Earth Planet. Sci. Lett.*, *308*, 359–368.

Takahashi, E. (1990), Speculations on the Archean mantle: Missing link between komatiite and depleted garnet peridotite, *J. Geophys. Res.*, *95*, 15,941–15,954.

Taylor, S. R., and S. M. McLennan (1985), *The Continental Crust: Its Composition and Evolution*, pp. 1–312, Blackwell Scientific, Oxford, U.K.

Taylor, S. R., and S. M. McLennan (1995), The geochemical evolution of the continental crust, *Rev. Geophys.*, *33*, 241–265.

Taylor, S. R., and S. M. McLennan (2009), *Planetary Crusts: Their Composition, Origin and Evolution*, 1–378, Cambridge Univ. Press, Cambridge, UK.

van der Hilst, R. D., S. Widiyantoro, and E. R. Engdahl (1997), Evidence for deep mantle circulation from global tomography, *Nature*, *386*, 578–584.

van Hunen, J., P. E. van Keken, A. Hynes, and G. F. Davies (2008), Tectonics of early Earth: Some geodynamic considerations, in *When Did Plate Tectonics Begin on Planet Earth?* edited by C. Condie, and V. Pease, pp. 157–170, Geological Society of America, Boulder, Colo.

Veizer, J., and S. L. Jansen (1979), Basement and sedimentary recycling and continental evolution, *J. Geol.*, *87*, 341–370.

Walzer, U., and R. Hendel (2008), Mantle convection and evolution with growing continents, *J. Geophys. Res.*, *113*, B09,405, doi:10.1029/2007JB005459.

Walzer, U., and R. Hendel (2009), Predictability of Rayleigh-number and continental-growth evolution of a dynamic model of the Earth's mantle, in *High Performance Computing in Science and Engineering '07*, edited by S. Wagner, M. Steinmetz, A. Bode, and M. Brehm, pp. 585–600, Springer, Berlin.

Wedepohl, K. H. (1995), The composition of the continental crust, *Geochim. Cosmochim. Acta*, *59*, 1217–1232.

Willbold, M., and A. Stracke (2006), Trace element composition of mantle end-members: Implications for recycling of oceanic and upper and lower continental crust, *Geochem. Geophys. Geosys*, *7*, Q04,004, doi:10.1029/2005GC001005.

Yamazaki, D., and S.-I. Karato (2001), Some mineral physics constraints on the rheology and geothermal structure of the Earth's lower mantle, *Am. Min*, *86*, 385–391.

Yoneda, A., M. Osako, and E. Ito (2009), Heat capacity measurement under high pressure: A finite element method assessment, *Phys. Earth Planet. Int.*, *174*, 309–314.

Zheng, Y. F., and S. B. Zhang (2007), Formation and evolution of Precambrian continental crust in South China, *Chinese Sci. Bull.*, *52*, 1–12.

Zindler, A., and S. Hart (1986), Chemical geodynamics, *Annu. Rev. Earth Planetary Sci.*, *14*, 493–571.